Early age deformations of concrete with high content of mineral additions

Aveline Darquennes, Muhammad Irfan Ahmad Khokhar, Emmanuel Rozière, Ahmed Loukili, Frédéric Grondin, Stéphanie Staquet

Early age deformations of concrete with high content of mineral additions

A. Darquennes [a], M.I.A. Khokhar [a,b], E. Rozière [a], A. Loukili [a,*], F. Grondin [a], S. Staquet [b]

[a] Research Institute of Civil Engineering and Mechanics (GeM), UMR CNRS 6183, Ecole Centrale de Nantes – 1 rue de la Noë, BP 92101, 44321 Nantes Cedex 3, France [b] BATir Department, Université Libre Bruxelles (ULB), 87 Avenue A. Buyl, 1050 Brussels, Belgium

Under the project "EcoBéton" (Green concrete) funded by the French National Agency (ANR), concrete mixtures with a high quantity of mineral additions, such as blast furnace slag and fly ash were studied. A first approach to quantify their cracking risk was to measure their plastic shrinkage evolution. In parallel, the evolution of other parameters such as setting, capillary depression and porosity were also monitoring to relate this deformation to the evolution of the microstructure of the studied mixtures. Setting monitoring by means of ultrasonic measurements allows obtaining significant macroscopic information such as hardening process and rigidity evolution. The correlation between these different parameters shows that the plastic shrinkage evolution can be divided into three phases driven by different mechanisms. Moreover, it appears that the use of mineral additions has an effect on the plastic shrinkage behaviour, but this impact is not proportional to the percentage of additions. It depends on the hydration process and the microstructure of the cementitious materials. So, it seems that an optimum content of cement replacement by mineral additions must be sought to limit the development of plastic shrinkage of concretes with mineral additions at early age. However, a high rate of substitution of cement may affect the early age compressive strength of the concrete. So these mixtures were also optimised to obtain a significant compressive strength at early age, but this optimisation leads to a higher risk of cracking for some of them.

1. Introduction

The clinkerisation of the constituent materials of cement requires high energy consumption and release of carbon dioxide. Since the Kyoto Protocol, cement industries tend to reduce the greenhouse gas emissions during cement manufacturing, especially from decarbonation of limestone. One solution proposed to this problem is replacing a part of cement by materials which do not alter the properties of concrete. Generally, these substitution materials are mineral additions such as fly ash and blast furnace slag, which are considered as industrial waste. However, the prescriptive requirements of the French Standard NF EN206 1 [5] puts limit on the use of mineral additions, when they are used during the concrete mixing. Higher mineral addition contents are allowed to use in concrete mixtures but their durability has to be shown according to the equivalent performance concept [18]. As a consequence this research project ANR EcoBéton aims to better understand the behaviour of concrete with high content of mineral additions. Under this research project, it has been shown that high rate of substitution of cement by mineral additions (fly ash, blast furnace slag and limestone filler) may affect the early age compressive strength of the concrete. To tackle this problem, these concrete mixtures with high rate of mineral additions were optimised using Bolomey's equation to have 2 day compressive strength (10 MPa at 20 °C) high enough to allow rapid removal of formwork [10]. Although this first approach gives quite satisfactory result from the view point of mechanical properties, its validation needs to take into account other properties of cementitious materials, such as durability and risk of cracking.

At very early age, the horizontal concrete elements such as slabs show a risk of cracking from the surface of fresh concrete soon after it is placed, following the development of plastic and drying shrinkage [7]. This risk of cracking depends on several parameters, such as the evolution of tensile stress, rigidity, shrinkage and relaxation of the material, and the restrained degree of deformations. In this study, a first approach to quantify the cracking risk of concretes with a high content of mineral additions was based on the monitoring of the evolution of plastic shrinkage at very early age. Other experimental techniques have also been used to assess the properties of concrete and explain the evolution of the plastic shrinkage. Besides understanding the phenomenon, this study shows the extent of influence of high content of mineral additions on the rate of evolution and the final value of the plastic

* Corresponding author.
E-mail address: ahmed.loukili@ec-nantes.fr (A. Loukili).

shrinkage. The same experimental approach was applied to concrete mixtures comprising a high content of mineral additions and optimised in terms of their mechanical performance.

2. Experimental techniques

Plastic shrinkage development was measured using a device developed at GeM laboratory of Ecole Centrale de Nantes [20]. In parallel to this deformation measurement, the evolution of hydration reaction and rigidity of the material was monitored continuously by means of ultrasonic measurements through a concrete specimen. This information is useful to better understand the plastic shrinkage behaviour in combination with the evolution of the microstructure of the material. In addition, other experimental techniques, i.e. measurement of mass loss and capillary depression, have also been implemented to quantify the mechanisms responsible for this deformation and to explain the effect of mineral additions.

2.1. Plastic shrinkage

The device for measuring the development of plastic shrinkage (Fig. 1) consists of a prism-shaped steel mould ($70 \times 70 \times 280\ mm^3$) whose inner walls are covered with Teflon. Concrete were cast in an envelope formed by two PVC plates ($70 \times 68 \times 5\ mm^3$) named reflecting plates, attached to a plastic sheet and positioned in the mould; this later was powdered with talc in order to limit friction between concrete and walls of the mould. Both ends of the mould were pierced in the centre to have a circular opening in order to monitor the movement of reflecting plates anchored to the ends of the specimen using two laser sensors. These sensors have an accuracy of about 2 μm. The specimen temperature was controlled by a water circulation in the side walls and the bottom of the steel mould, thus the concrete samples have been kept in the conditions similar to isotherm. However, the temperature of concrete was also monitored using a thermocouple placed in the concrete specimen. In this study, the tests were performed at 20 °C and 50% RH, and they showed good repeatability (Fig. 2), with a difference of 40 μm/m between the final values of the plastic shrinkage of two tests performed on the same composition. Tests started about 20–30 min after adding water during the mixing process. All data (plastic shrinkage, temperature, mass loss, setting time and capillary depression) were logged on a computer every 10 min for a period of 24 h.

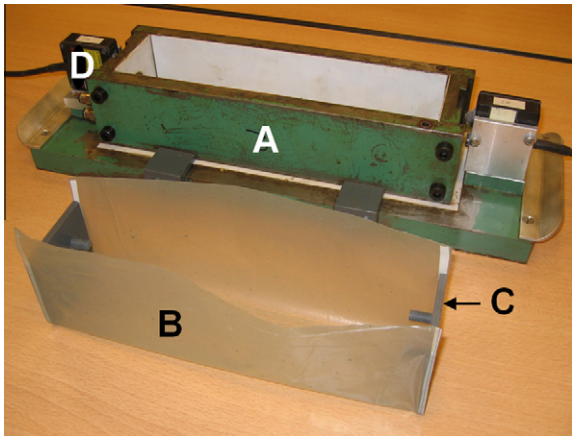

Fig. 1. Plastic shrinkage measuring device (A: mould, B: plastic sheet, C: reflecting plates made of PVC, D: laser sensor).

2.2. Mass loss

Water loss was monitored for all the mixtures using a cylindrical sample ($Ø = 100$ mm and $h = 70$ mm) subjected to the same environmental conditions as the concrete specimen used for measuring plastic shrinkage. Only the upper surface of the specimen was subjected to drying conditions. From this test, the rate of evaporation of water can be determined by dividing the mass loss by the surface of the cylinder.

2.3. Capillary depression

The evolution of the capillary depression in the concrete was measured as shown in Fig. 3, using a porous ceramic cup placed horizontally at mid-height of a cylinder [13]. Its dimensions were identical to those of the specimen used for measuring the mass loss. Ceramic cup was connected to pressure sensor using a thin tube.

2.4. Setting

The ultrasonic velocity measurements were used to monitor the setting of the material at early age using the FreshCon device developed at University of Stuttgart [14] (Fig. 4).This device is constituted of two polymethacrylate (PMMA) walls 5.9 cm apart and held by four screws. The mould is U-shaped foam with

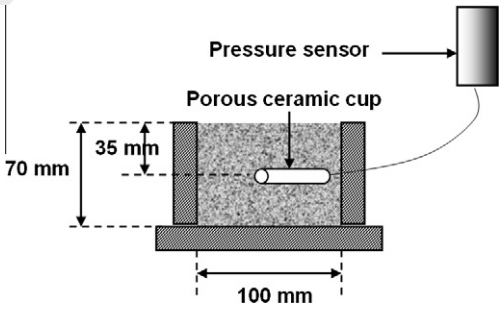

Fig. 3. Schematic section view of set up for measurement of capillary depression.

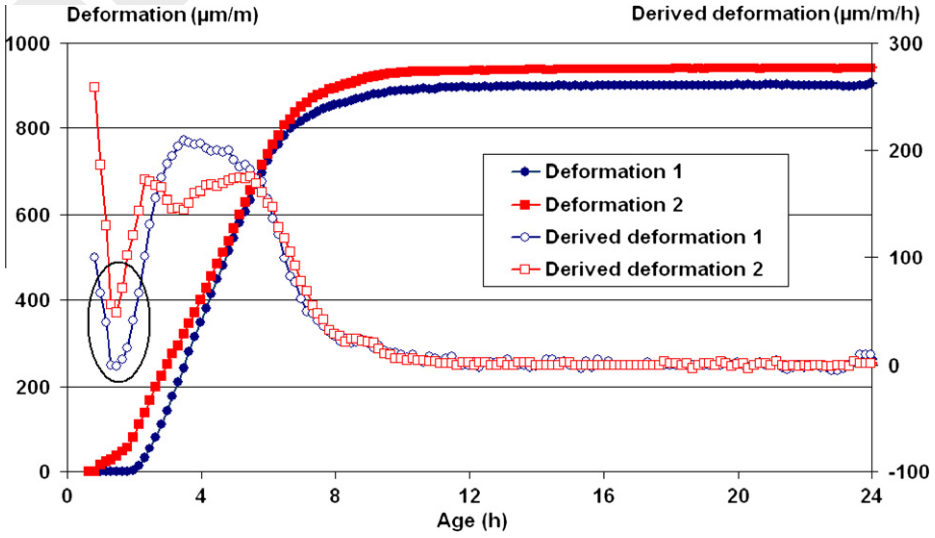

Fig. 2. Deformation evolution of 75GGBS and its derivatives for two trials.

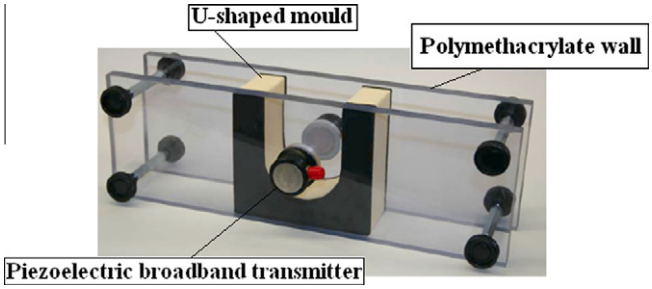

Fig. 4. Mould of FreshCon device.

high damping properties to absorb the waves through the mould and travelling around the concrete specimen (concrete volume of 450 cm^3). A pulse signal with a width of 2.5 µs of which the amplitude was enhanced by an amplifier was generated at selected regular intervals during this test. The ultrasonic longitudinal compression waves were then transmitted through the concrete sample by means of a piezoelectric broadband transmitter. The signal was received by an ultrasonic receiver after travelling through the sample and sent back to the data acquisition card (DAQ card). During the test, ultrasonic velocity, energy and frequency spectrum evolution are computed by the FreshCon software. The test was carried out in an air-conditioned room at 20 °C and the sample was protected by a plastic foil against desiccation phenomena and risk of decoupling between concrete and mould walls following the development of drying shrinkage. During the test, changes in ultrasonic velocity were measured continuously and used to determine two parameters: initial and final setting. According to Robeyst et al [15], the initial setting corresponds to the time of the first inflection point on the velocity curve determined mathematically by calculating the derivative of the velocity curve. This inflection point corresponds to the moment when the cement particles are connected [21]. The final setting appears when the growth rate of velocity decreases sharply (= the time when the first derivative of the velocity curve tends to zero). The terms of initial and final setting as defined in standards such as ASTM C403 are used to describe arbitrarily chosen stages of setting in practice [11], while the ultrasonic method gives a more complete picture of the setting process.

2.5. Porosity

Capillary porosity and pore size distribution of concrete were quantified using a mercury porosimeter (Autopore IV Micrometrics 9510), which can detect pores with diameters ranging from 360 µm to 0.003 µm. However, such measurements can only quantify the pores accessible to mercury and lead to a wrong estimation of the pore size distribution of the cementitious material. Majority of the pores are located in the interior of the specimen, and most of them can be reached by mercury only through a long percolative chain of intermediate pores of varying sizes and shapes [4]. So this experimental technique tends to underestimate the amount of large pores. In these experiments, measurements were made on samples of mortar at 1 day collected from concrete to limit the effect of aggregate porosity on measurements. While interpreting these tests, the capillary porosity of the material has been considered within the interval characterized by pore diameters between 5 and 0.01 µm.

3. Materials

In these tests, the concrete mixtures were made of a Portland cement (CEM I 52.5 N CE CP2 NF), crushed coarse aggregate (10/14 and 6/10 mm) and sea sand (0/4 mm), a polycarboxylate type superplasticizer in addition to the mineral additions like blast furnace slag and fly ash. Physical properties of these last constituents are detailed in Table 1. These mineral additions were used with different contents: 50% and 75% of blast furnace slag for 50GGBS and 75GGBS respectively and 50% of fly ash for 50FA (Table 2).

Table 1
Physical properties of the cementitious materials.

	Cement CEM I	GGBS	Fly ash
Density (g/cm^3)	3.11	2.89	2.24
Blaine (m^2/kg)	340	462	405
Passing 45 µm (%)	/	/	19.94
SO_3	3.3	0.1	0.64

Tests were carried out at 20 °C for two different classes of composition: non optimised concrete mixtures (50GGBS, 75GGBS and 50FA) and optimised concrete mixtures (50GGBSOpt, 75GGBSOpt and 50FAOpt) (Table 2). Non optimised mixtures are characterized by identical effective water content, volume of paste and granulometric curve. While in case of optimised mixtures, these parameters were modified to obtain a compressive strength equal to 10 MPa at 2 days. Therefore, optimised mixtures are characterized by lower w/b and w/c ratios, higher cement content, lower water content, volume of paste equal or higher than non optimised mixtures. Moreover, optimised mixtures contained a larger quantity of superplasticizer than non optimised mixtures.

4. Experimental results

4.1. Description

Fig. 5 shows the evolution of plastic shrinkage of CEM I and non optimised mixtures with mineral additions. Directly after the start of measurement (about 30 min after the water cement contact), deformation of CEM I began to increase. After 2 h, the increase rate of deformation slowed down before rising again. From that moment, CEM I is characterized by a linear increase in plastic deformation up to 5.3 h. Concretes with slag (50GGBS and 75GGBS) showed a similar pattern, but with a temporary delay. Their plastic shrinkage began to grow at 1.2 h and 0.8 h respectively. This development was rather slow during the first 2 h, and then evolved linearly until 6 h and 7 h for 50GGBS and 75GGBS respectively. However, the final value of 75GGBS is three times higher than that of 50GGBS. For 50FA, no deformation was registered during the first 3 h. Then, the deformation gradually evolved until 9 h reaching a value of plastic shrinkage close to that of 50GGBS (about 300 µm/m). Moreover, for all mixtures, the temperature of the specimen was maintained at about 20 °C thanks to temperature regulation system of the mould (Fig. 5).

Plastic shrinkage development of different concrete mixtures showed a particular behaviour during the first hours after placement of the concrete. This can be attributed to several phenomena that occur within the fresh material. In fact, the material has undergone a rearrangement of its constituents due to gravity, when the solid particles settled down. During this consolidation process, some water percolated onto surface and it forms a water film on the surface of the concrete specimen (bleeding water), which can evaporate. In addition, chemical shrinkage would also occur when the cement comes into contact with water. After this first phase, drying shrinkage phenomenon was predominant in deformation of concrete specimen. Initially, the beginning of the predominance of drying shrinkage over plastic shrinkage seems to appear at a moment characterized by an increase in the rate of plastic shrinkage, which corresponds to the first minimum of the derivative of the plastic shrinkage values (Fig. 2). This treatment of experimental data allowed us determining clearly the impact of mineral additions on the amplitude of plastic shrinkage (Fig. 6), delaying lightly the initialization of the deformation. With initialization of the shrinkage curves at this point, it appears that the behaviour of concretes with 50% of blast furnace slag and 50% of fly ash is similar in both the rate of increase in the deformation and its final value. Moreover, the rate of shrinkage for CEM I and 75GGBS tends to be similar, but their final values are different. Finally, this analysis shows that the mixture with 75% slag content is characterized by the highest shrinkage value at 24 h. In addition, the addition of blast furnace slag does not generate systematically an increase in plastic shrinkage, since its value for 50GGBS is lower than that of CEM I.

Table 2
Compositions of the optimised and non-optimised mixtures.

	CEM I	50GGBS	50GGBSOpt	75GGBS	75GGBSOpt	50FA	50FAOpt
Composition (kg/m^3)							
Cement	303	146	163	72	103	126	174
Blast-furnace slag	/	146	163	215	309	/	/
Fly ash	/	/	/	/	/	126	174
W_{eff}[a]	182	182	171	182	170	182	170
Sand 0/4	855	855	855	855	817	855	824
Gravel 6/10	211	211	211	211	202	211	203
Gravel 10/14	875	875	875	875	836	875	843
Superplasticizer	1	1	1.6	0.9	2.8	0.8	2.2
Characteristics							
w/b[b]	0.60	0.62	0.52	0.63	0.41	0.72	0.49
w/c[c]	0.60	1.25	1.05	2.54	1.65	1.45	0.98
V_{paste}[d] (l/m^3)	279	279	279	280	310	279	304
V_w/V_b[e]	1.868	1.868	1.573	1.866	1.214	1.868	1.260
$f_{c,\,2}$ (MPa)	29.6	8.0	12.5	3.3	12.0	4.8	12.4
$f_{c,\,28}$ (Mpa)	49.1	33.4	39.1	33.4	53.8	11.7	30
Slump (mm)	170	150	170	160	170	170	200

[a] $W_{eff} = w_{added} + w_{superplasticizer} - w_{absorbed\ by\ aggregates}$.
[b] w/b = water to binder ratio.
[c] w/c = water to cement ratio.
[d] V_{paste} = Volume of paste.
[e] V_w/V_b = Volume of W_{eff} to Volume of binder ratio.

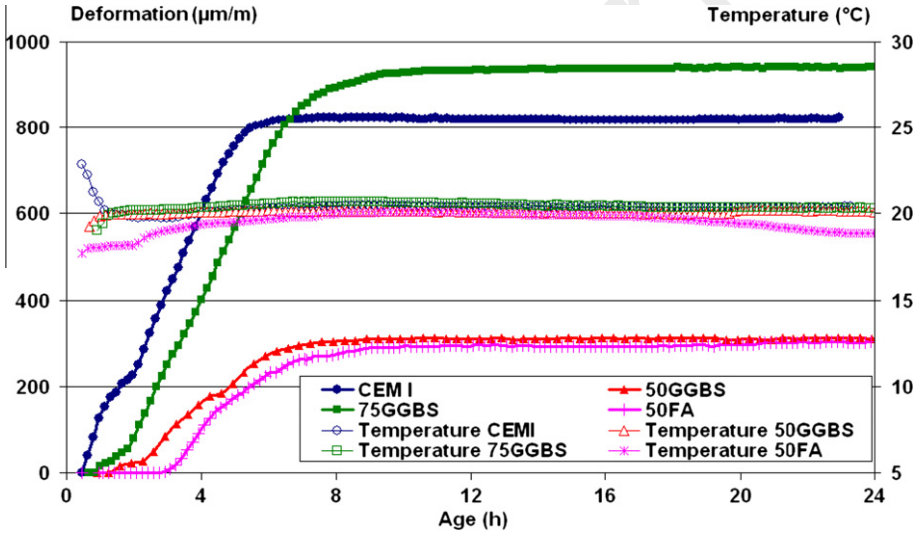

Fig. 5. Evolution of plastic shrinkage and temperature of non-optimised mixtures (raw curves).

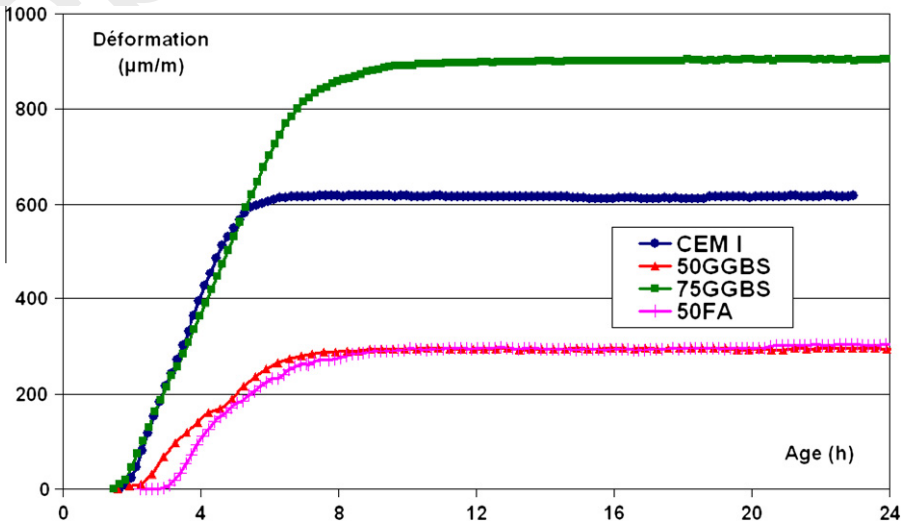

Fig. 6. Evolution of the plastic shrinkage initiated at the first minimum of the first derivative of the plastic shrinkage curve for the non-optimised mixtures.

4.2. Correlation

To understand the phenomena occurring during the plastic shrinkage development, evolution in the capillary depression, ultrasonic velocity, mass loss and temperature were analyzed for all the studied mixtures. First, it appeared that for all non optimised compositions (Figs. 7–9), the raw curve of plastic shrinkage could be divided into three phases.

4.2.1. The first phase

This phase occurs between the water–cement contact and the moment characterized by the appearance of a negative capillary depression reflecting the appearance of menisci in the pores of the cement matrix located near the ceramic porous sensor. This moment coincides quite well with the appearance time of the minimum of first derivative of the plastic shrinkage (Fig. 2). During this first phase, an increase in ultrasonic velocity through a concrete specimen can be observed. It occurs well before the initial setting. At this age, the material is in a semi fluid state and it has no rigid structure holding together its constituent materials. Thus, the increase in ultrasonic velocity is probably due to a rearrangement of the material under the gravity. This phenomenon can reduce the distance between the particles and thus enhance the propagation of compression waves through the material. During this period, Voigt et al [21] also observed the formation of ettringite around cement particles. These hydration products do not create connected particles and have no or little influence on the stiffening process. However, they fill pore spaces as a result of which the porosity and the air content decrease and the velocity increases. This initial value of velocity can also be attributed to the presence of air entrained during the mixing procedure [9]. Moreover, the determination of the signal onset time and the wave velocity is less accurate during this early period (repeatability error of 10%) due to larger signal attenuation compared to a more hard

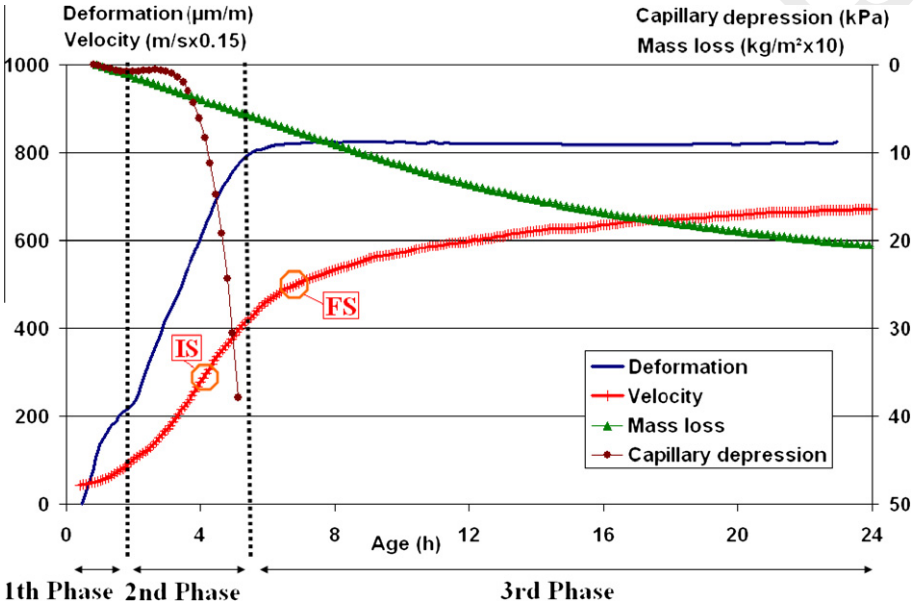

Fig. 7. Evolution of shrinkage, mass loss, temperature, ultrasonic velocity and capillary depression for CEM I (IS = initial setting and FS = final setting).

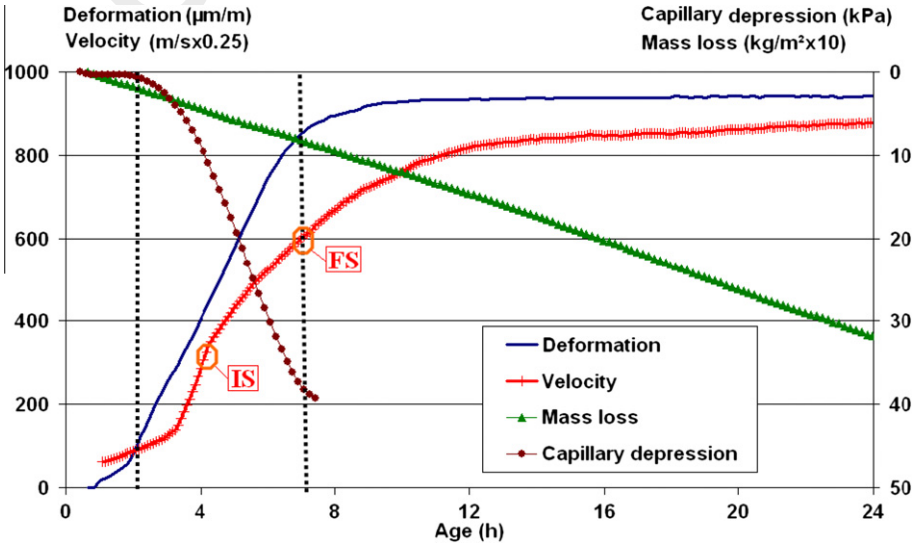

Fig. 8. Evolution of shrinkage, mass loss, temperature, ultrasonic velocity and capillary depression for 75GGBS (IS = initial setting and FS = final setting).

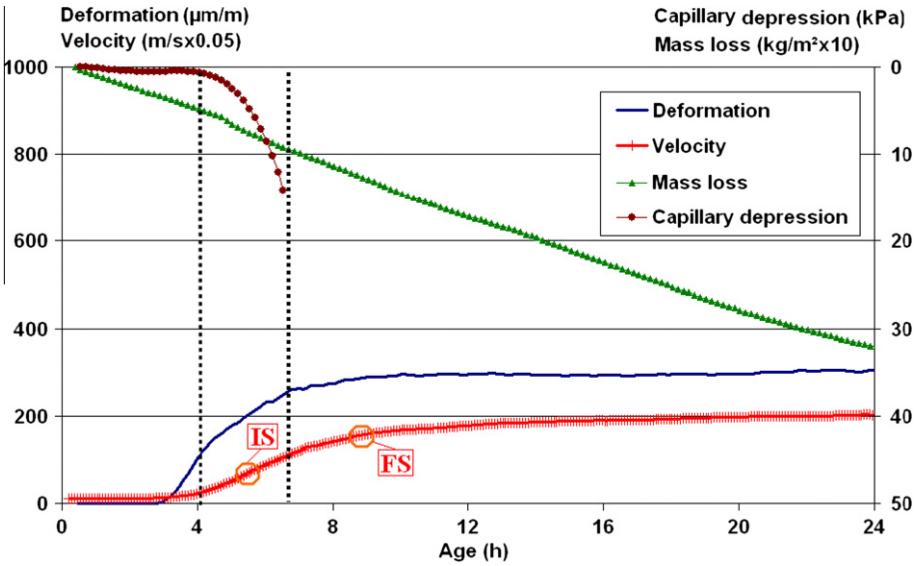

Fig. 9. Evolution of shrinkage, mass loss, temperature, ultrasonic velocity and capillary depression for 50FA (IS = initial setting and FS = final setting).

ened material (repeatability error of 1.0 1.5%) [16]. During the consolidation of the material, concrete water percolates onto the surface and a layer of water called bleeding water forms. This phe nomenon seems to have occurred for all studied mixtures. In fact, during the first hours after the contact of cement with water, its evaporation rate is similar for all mixtures (Fig. 10) and it is close to that of open water. Thus, the evaporation rate of water at a very early age is not influenced by the type of material. However, although the drying shrinkage can only be developed within the material from the time when the bleeding water evaporates more quickly to the surface it appears, a linear shrinkage has even been measured during this phase. This deformation may be caused by rearrangement of the material under the gravity and due to chem ical shrinkage. In fact, this last deformation could begin because of the formation of hydration products around the cement grains.

4.2.2. The second phase

With the advancement of hydration reaction, a skeleton of hy drates is formed gradually in the cement matrix. The formation of hydrates partially filling the pore spaces previously occupied by the water facilitates the propagation of compression waves through the material due to the increased content of solid compo nents. This phenomenon is reflected by the increase in ultrasonic velocity. Menisci appear gradually between the solid grains and capillary depression increases for all studied mixtures, except for 50FA. This capillary depression generates stresses on the solid skel eton which tends to shrink. From that moment, the deformation rate increased for all studied mixtures. From the initial setting, a moment located near the inflection point of the capillary depres sion curve (Table 3), the evolution rate of the capillary depression increases significantly and generates an increase in plastic shrink age. According to the Laplace's equation (Eq. (1)), increase in the capillary depression is due to decrease in pore size caused by in creased hydrates. From that moment, the kinetics of plastic shrink age seems linked to capillary depression, since the value of these two parameters increased simultaneously.

$$P_l \quad P_g \qquad \frac{2\sigma}{r}\cos(\theta) \tag{1}$$

where θ is the wetting angle, r is radius of the pore containing the meniscus and σ is the surface tension of the liquid.

End of the second phase is linked to the change of slope of the plastic shrinkage curve characterizing a progressive decrease in its rate. This behaviour is probably due to an increase in material rigidity, since this moment is near to the final setting of the mate rial. It is also close to the time when the capillary depression stopped measuring, means to say when the sensor ceases to be in contact with the liquid phase of the capillary water. However, the time when the capillary depression stopped measuring is not an intrinsic feature of the material and it depends partly on the characteristics of the sensor for measuring capillary depression.

4.2.3. The third phase

During this phase, kinetics of plastic shrinkage decreases and eventually vanishes due to significant material stiffness at this age. An estimation of the evolution of the material stiffness can be determined from the Eq. (2) suggested by the [1]. This equation is characterized by two parameters, the Poisson coefficient and the density, which vary with the advancement of hydration. But they were taken as constant and equal to 0.2 and 2400 kg/m^3 respec tively. Moreover, this relation is only valid for a solid material. In fact, increase in the ultrasonic velocity beyond the final setting shows that the rigidity of the material is increasing and becomes significant with the progress in the hydration reaction (Fig. 11). It may therefore oppose to the plastic shrinkage and cancel its evolu tion. Thus, the final setting may be considered as the time when the material begins to develop a significant rigidity and can resist its internal deformation. In this case, it can be treated as time zero, defined as the moment from which internal stresses may develop in the heart of the material [3].

$$E_d \quad V^2 \frac{\rho(1+\upsilon)(1 \quad 2\upsilon)}{(1 \quad \upsilon)} \tag{2}$$

where E_d is the dynamic elastic modulus (Pa), V is ultrasonic veloc ity (m/s), υ is Poisson coefficient and ρ is the density (kg/m^3)

5. Discussion

5.1. Impact of mineral additions

Fig. 5 shows that the concrete mixture with 50% of mineral additions is characterized by the lowest value of plastic shrinkage at 24 h, while 75GGBS is characterized by the highest shrink

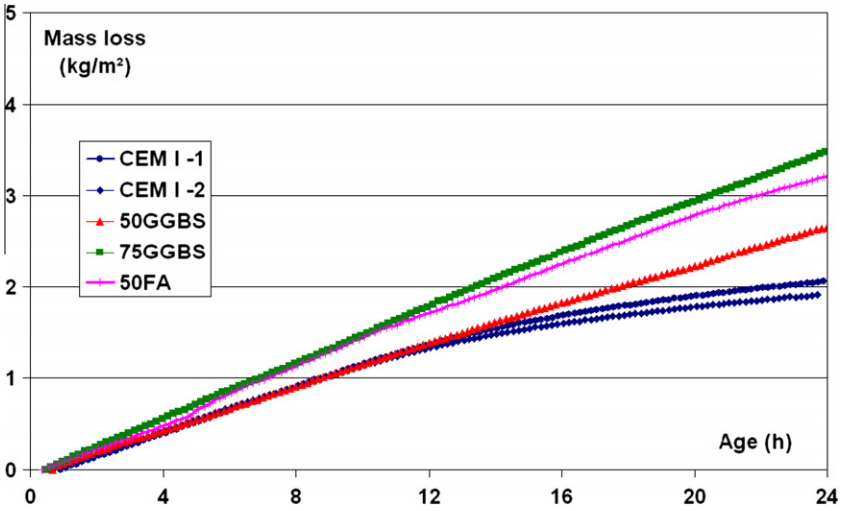

Fig. 10. Evolution of the mass loss in the non-optimised mixtures.

Table 3
Moment of appearance of the inflexion point of capillary depression and initial setting time of the non-optimised mixtures.

Compositions	Inflexion point of capillary depression (h)	Initial setting time (h)
CEM I	4.80	4.17
50GGBS	4.75	3.23
75GGBS	5.58	4.00
50FA	6.22	5.53

age. Thus, this mixture possesses an actual risk of cracking because of the development of its plastic shrinkage. Its deformation reaches 860 μm/m at 24 h, a value close to that proposed in the literature [8] to characterize the high risk of cracking of the material (1000 μm/m).

After the first phase dominated by the phenomena of putting the material in place, evaporation and chemical shrinkage, plastic shrinkages of CEM I and 75GGBS show similar kinetics (Fig. 6). However, plastic shrinkage of CEM I reached its final value earlier than 75GGBS. This behaviour is probably due to the rapid setting of this material (Table 4). So, its cement matrix attains rapidly a significant rigidity.

Analysis of the Figs. 7–9 shows that the plastic shrinkage development during the concrete setting process seems to be directly linked to the evolution of the capillary depression because of their linear growth. From this observation, it would seem logical that increase in the capillary depression of CEM I and 75GGBS is similar, because their deformation kinetics tends to be similar during setting. However, the development of their capillary depression (Fig. 12) differs by their initialization times (2.4 h and 3.1 h for 75GGBS and CEM I respectively) and their kinetics. This early initialization of the capillary depression for 75GGBS can be explained by its rapid initial setting (Table 4), a phenomenon that may be associated with the existence of a path of interconnected and hydrated binder particles allowing the appearance of capillary pores in the cement matrix. This rapid hydration initialization of 75GGBS is probably due to its large *w*/*c* ratio. Thus a larger amount of water is available for the hydration of the clinker particles of this concrete and their hydration can begin earlier. This behaviour allows accelerating the beginning of the slag hydration since its hydration depends on its dissolution by the hydroxyl ions released during the clinker hydration [12].

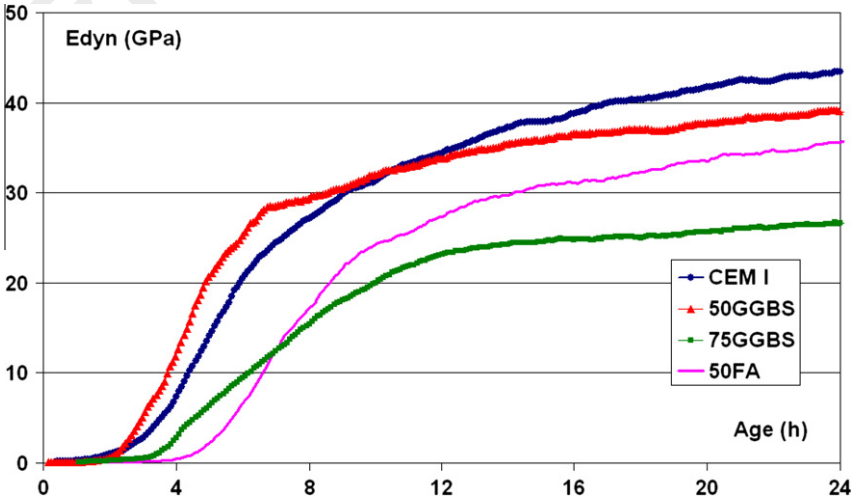

Fig. 11. Evolution of the dynamic elastic modulus in the non-optimised mixtures.

Table 4
Initial and final setting time determined by the evolution of ultrasonic velocity.

Compositions	Initial setting (h)	Final setting (h)
CEM I	4.17	6.83
50GGBS	3.23	5.45
50GGBSOpt	4.13	7.64
75GGBS	4.00	7.08
75GGBSOpt	3.60	7.82
50FA	5.53	8.85
50FAOpt	7.10	11.67

The difference in kinetics of the capillary depression development can be explained by the pore structure and the rate of evaporation of CEM I and 75GGBS. In fact, these last are the driving parameters of the capillary depression development for concretes subjected to desiccation [19]. CEM I is characterized by a slow evaporation rate during the second phase (Fig. 10) and a lower and finer porosity than 75GGBS (Figs. 13 and 14). Thus, the intensity of the capillary depression of CEM I is amplified by the lowest pore size of its main population (Table 5) compared to that of 75GGBS. Capillary depression is inversely proportional to the pore diameter according to the Laplace's equation (Eq. (1)). Porous structure of 75GGBS is coarser simply due to its low content of hydrates in the cement matrix, because of the initial slow reaction of its hydration [2].

Viewing these differences in behaviour of the capillary depression of CEM I and 75GGBS, it appears that it is not the only factor driving the plastic shrinkage evolution. This observation seems to be confirmed by the presence of a linear relationship between the plastic shrinkage and evaporation rate during the second phase (Fig. 15). Thus, the combination of these two phenomena could explain the similar rate of development of plastic shrinkage of CEM I and 75GGBS during the second phase.

In the end, the final value of the plastic shrinkage of 75GGBS is higher than that of CEM I despite its coarser porosity and its slow rate of increase in capillary depression. Two explanations may be suggested to understand this observation. The first is the slow hydration reaction of 75GGBS delaying the increase in its rigidity and the appearance of its threshold value from which the plastic shrinkage does not evolve anymore. The second is related to the porous structure of the material. The low capillary depression

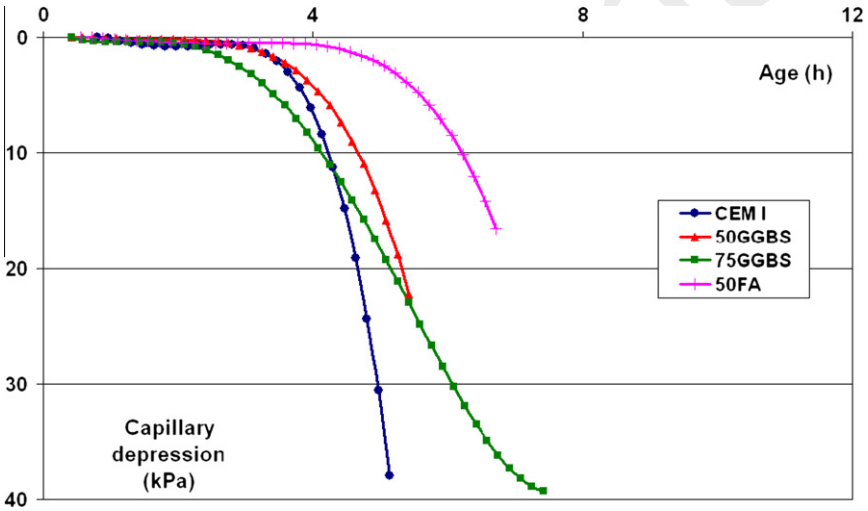

Fig. 12. Evolution of the capillary depression in the non-optimised mixtures.

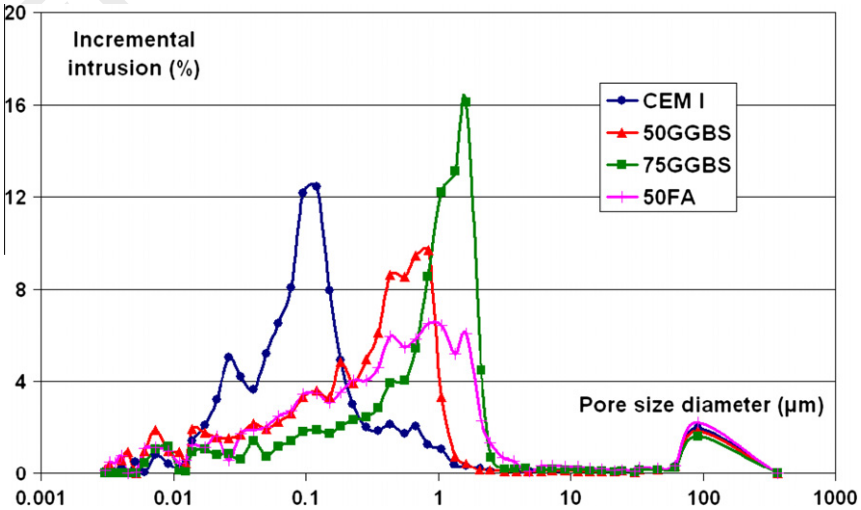

Fig. 13. Pore size distribution for non-optimised mixtures.

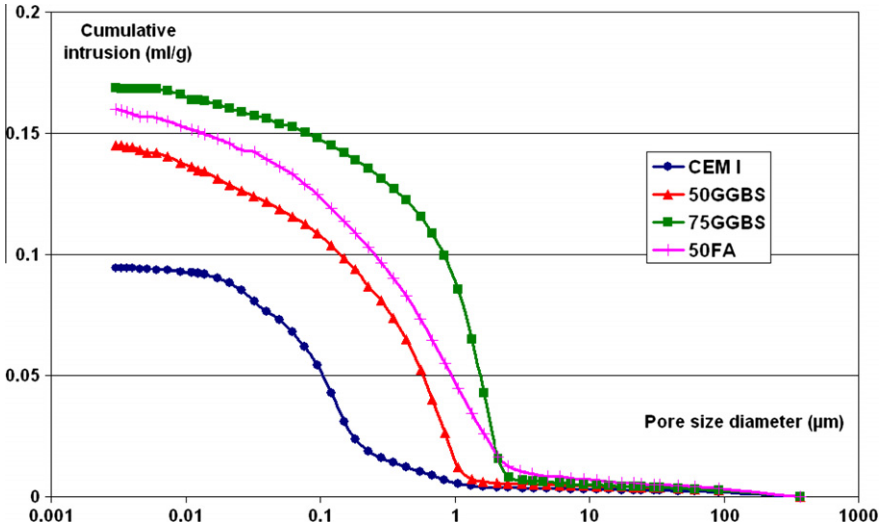

Fig. 14. Cumulative porosity for non-optimised mixtures.

Table 5
Capillary porosity and population of main pores.

Compositions	Capillary porosity (%)	Penetration threshold (µm)	Population of main pores (µm)
CEM I	16.2	1.04	0.121
50GGBS	25.5	1.31	0.835
50GGBSOpt	20.4	0.68	0.435
75GGBS	26	2.53	1.610
75GGBSOpt	21.1	1.33	0.434
50FA	26.8	3.08	0.837
50FAOpt	21.1	0.83	0.432

occurring in the large pores of 75GGBS could be compensated by its high total capillary porosity (Table 5). The large capillary pores content of 75GGBS reflects a larger connectivity between its pores than that of CEM I. So, the rate of evaporation is larger for 75GGBS than for CEM I (Fig. 10). Finally, this analysis shows that differences in behaviour between CEM I and 75GGBS are mainly due to the advancement of their hydration and their porous structure.

Mixtures with 50% of mineral additions (50GGBS and 50FA) are characterized by a quasi similar evolution of their plastic shrinkage during the second phase and a same final value at 24 h (Fig. 6). However, the development of capillary depression is not quite similar (Fig. 12). The initialization of the deformation and its rate is later and slower respectively for 50FA than for 50GGBS. This difference in behaviour is probably related to slow hydration reaction of 50FA due to its pozzolanic reaction. Its initialization strongly depends on the alkalinity of the aqueous solution of the pores. However, the alkalinity of pore solution grows slowly and can take up to several days [6]. This delayed hydration development is confirmed by the presence of larger pores within the cement matrix for 50FA than for 50GGBS viewing its larger penetration threshold value (Table 5). However, their main pore population and volume of capillary pores tend to be similar (Table 5). Moreover 50FA, which is characterized by a higher rate of evaporation (Fig. 10), can accelerate the drying shrinkage at the surface of the specimen and increase plastic shrinkage. However, the linear evolution of plastic shrinkage with reference to mass loss is less pronounced for the two mixtures with 50% of mineral additions (Fig. 15).

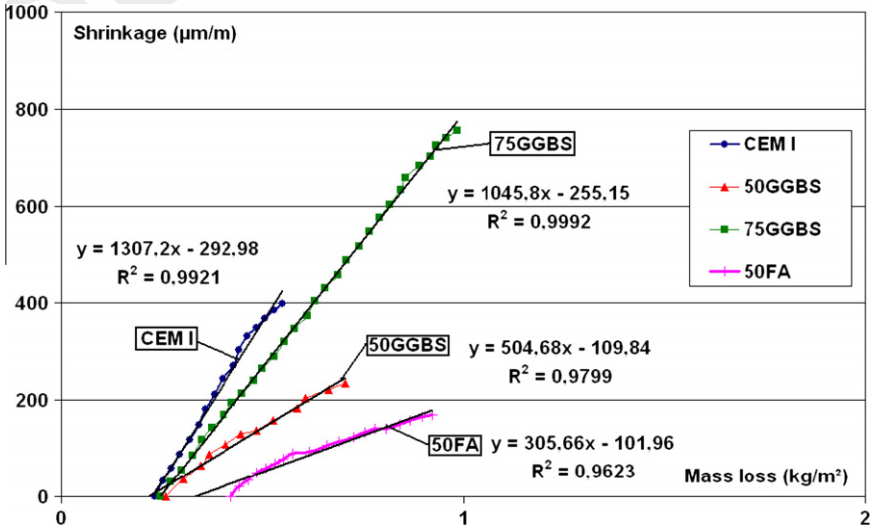

Fig. 15. Evolution of shrinkage as function of mass loss during the second phase.

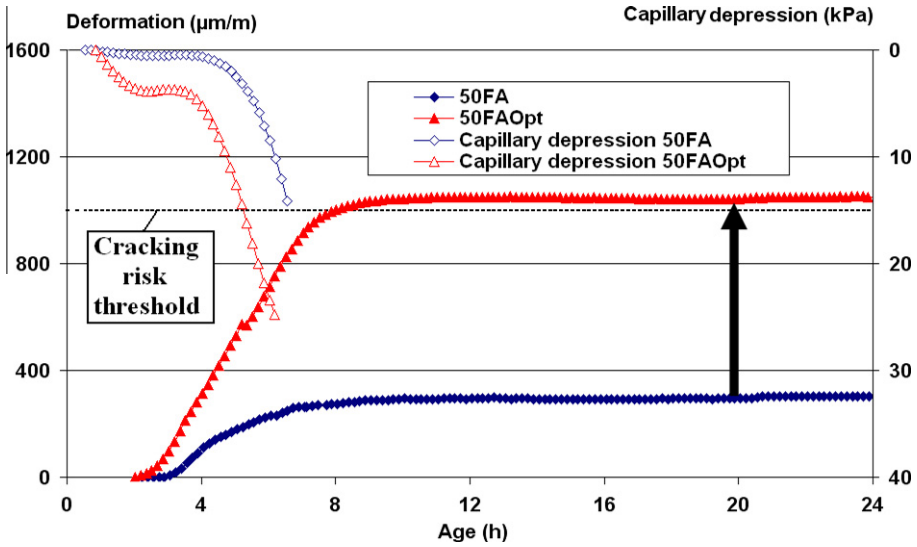

Fig. 16. Evolution of the plastic shrinkage initiated at the first minimum of the first derivative of the plastic shrinkage curve for the mixtures with 50% of fly ash.

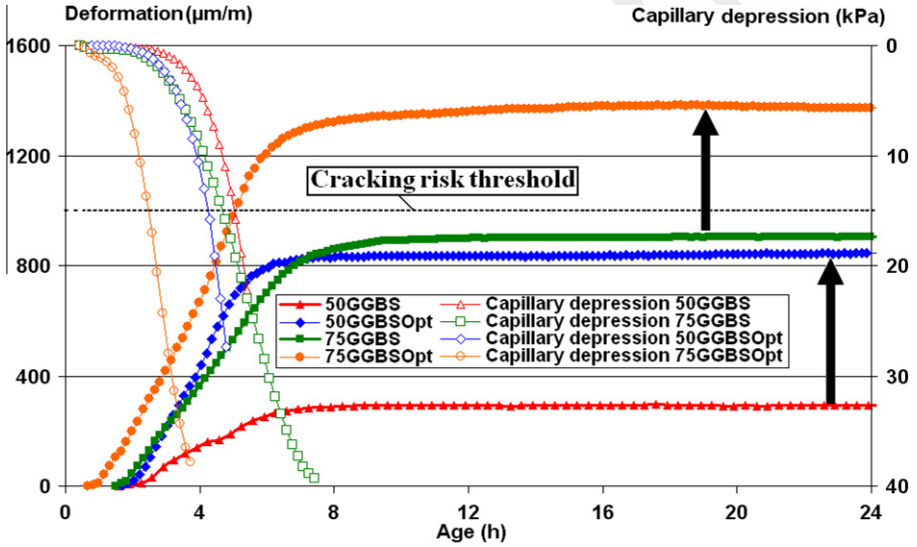

Fig. 17. Evolution of the plastic shrinkage initiated at the first minimum of the first derivative of the plastic shrinkage curve for the mixtures with 50% and 75% of slag.

5.2. Optimised mixtures

Compared to concrete mixtures with mineral additions presented previously, the optimised mixtures (Table 2) are characterized by higher cement content, lower w/c and w/b ratios, and same or higher volume of paste. The variations of these parameters directly influence the behaviour of the plastic shrinkage of these mixtures, since their hydration reaction development (Table 4) and their porous structure (Table 5) are modified.

Four changes can be observed in the evolution of plastic shrinkage of optimised mixtures compared to non optimised mixtures (Figs. 16 and 17): acceleration of initialization of plastic shrinkage, increase in its evolution rate, duration of the second phase and its final value.

Acceleration of the initialization of plastic shrinkage can be attributed to the decrease in pore size of the optimised mixtures leading to an increase in capillary depression (Eq. (1)), hence accelerating the appearance of the drying shrinkage. In fact, the optimised mixtures are characterized by a decrease in capillary porosity (Table 5), pore diameter characterizing the threshold of penetration (Figs. 18 and 19), as well as that of the main population of pores (Fig. 20 and Table 5). In addition, a lower w/b ratio also generates an accelerated chemical shrinkage.

Beyond the first phase, the plastic shrinkage evolves linearly as function of time and its growth rate has increased compared to non optimised mixtures. This observation is also valid for the capillary depression (Figs. 16 and 17) and can be also explained by the porous structure of these materials. The duration of this second phase is also longer for optimised mixtures. This behaviour is probably due to delayed final setting of these concretes (Table 4); these delays can be related to their higher content of superplasticizer.

Although these optimised mixtures have satisfactory mechanical properties, optimisation of the concretes with mineral additions does not allow to obtain a microstructure similar to CEM I (Figs. 18 and 19). Moreover, their ultimate value of plastic shrinkage is significantly higher than non optimised mixtures. Finally, it appears that 50FAOpt and 75GGBSOpt have a high risk of cracking, since the value of plastic shrinkage at 24 h is greater than 1000 µm/m (Figs. 16 and 17). This behaviour is probably related

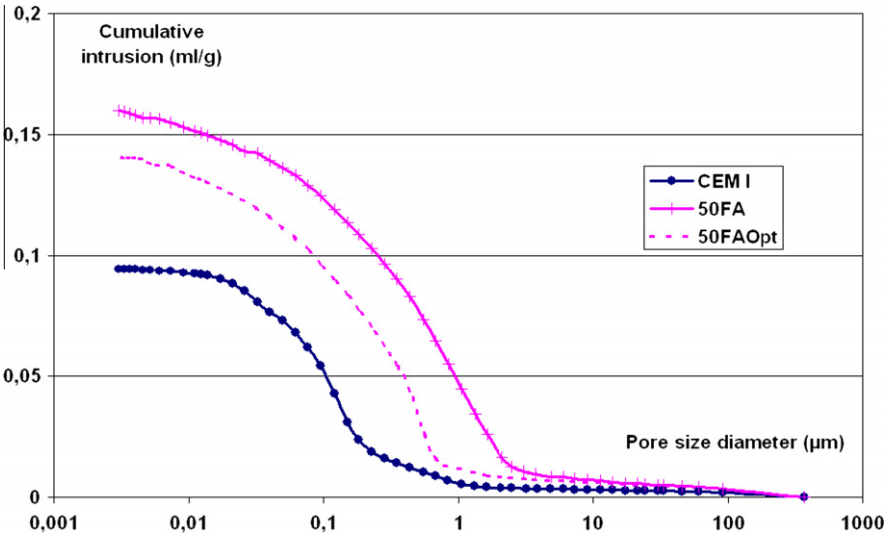

Fig. 18. Cumulative porosity of mixtures with 0% and 50% of fly ash.

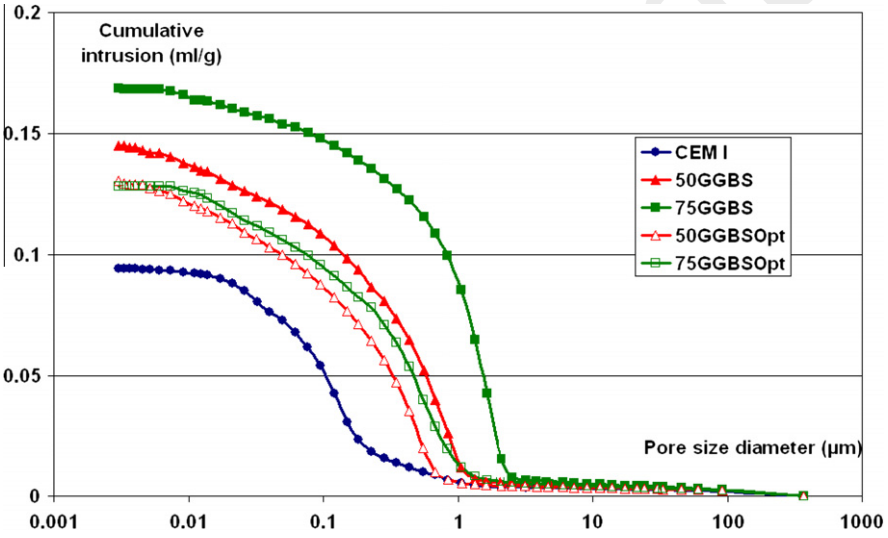

Fig. 19. Cumulative porosity of mixtures with 0%, 50% and 75% of slag.

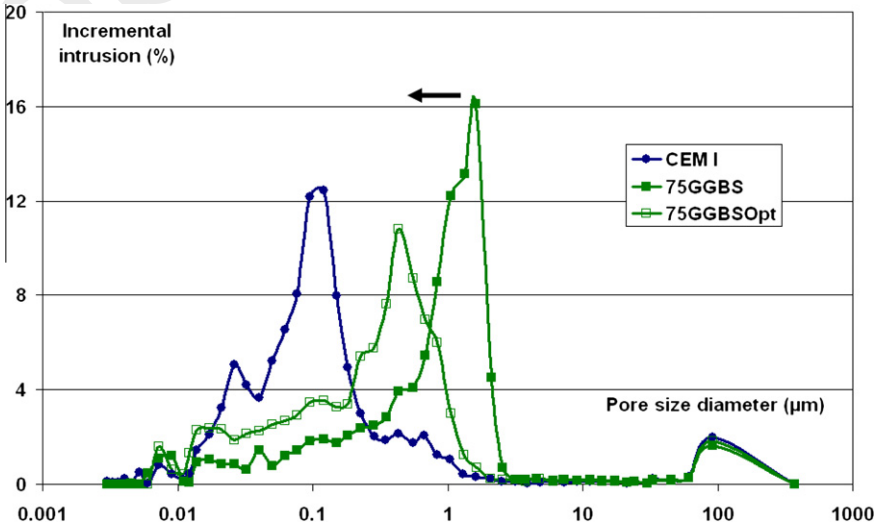

Fig. 20. Pore distribution of the mixtures with 0% and 75% of slag.

to the higher volume of paste of these mixtures (Table 2). According to Rozière et al [17], the drying kinetic tends to increase with the volume of paste.

6. Conclusions

This research allowed improving the knowledge about concrete mixtures with a high content of mineral additions at very early age by means of an in depth study on plastic shrinkage. An estimation of cracking risk at early age was also made based on the development of this deformation. Moreover, the plastic shrinkage was linked to the evolution of the material microstructure to understand the mechanisms responsible for this deformation and to explain the effect of mineral additions. The main conclusions of this study can be emphasized hereafter:

The concrete with a simple substitution of 75% of slag is characterized by the highest amplitude of plastic shrinkage, with a value close to 1000 μm/m. So, this mixture shows a relatively high risk of cracking. This behaviour is attributed to its slow hydration and its high capillary porosity.

The mixtures with 50% of mineral additions (fly ash or blast furnace slag) are characterized by a quasi similar evolution of their plastic shrinkage which is inferior to that of the reference mixture. So, the addition of blast furnace slag does not generate systematically an increase in plastic shrinkage. It seems that an optimum percentage of cement replacement by mineral additions must be sought to limit the development of plastic shrinkage of concrete with mineral additions at early age.

The optimisation of concrete mixtures to obtain a significant 2 day compressive strength leads to a higher amplitude of plastic shrinkage with a faster kinetics. This behaviour is linked to their finer porous network. But the optimisation of concrete mixtures with a high content of mineral additions also increases their cracking risk at early age (plastic shrinkage amplitude >1000 μm/m). The use of such compositions for horizontal surfaces susceptible to plastic shrinkage requires minimising the paste volume or an appropriate surface curing.

Acknowledgments

This research was achieved in the framework of the French research Project ANR/RGCU EcoBéton. The authors would like to extend their appreciation and gratitude for the financial support provided by the National Research Agency. Special Thanks to Dr P. Turcry for useful discussions and suggestions.

References

[1] ASTM-C597. Standard test method for pulse velocity through concrete; 1997.
[2] Baron J, Ollivier J-P. La durabilité des bétons. Presses de l'Ecole Nationale des Ponts et Chaussées; 1992. 453p.
[3] Bentur A. Early-age shrinkage and cracking in cementitious systems. Concr Sci Eng 2001;3:3–12.
[4] Diamond S. Mercury porosimetry–an inappropriate method for the measurement of pore size distributions in cement-based materials. Cem Concr Res 2000;30:1517–25.
[5] EN 206-1. Béton – Partie 1: Spécification, performances, production et conformité; 2004. 91p.
[6] Fraay ALA, de Haan YM. The reaction of fly ash in concrete. A critical examination. Cem Concr Res 1989;19:235–46.
[7] Henkensiefken R, Briatka P, Bentz DP, Nantung T, Weiss J. Plastic shrinkage cracking in internally cured mixtures. Concr Int 2010;32(2):49–54.
[8] Holt E, Leivo M. Cracking risks associated with early age shrinkage. Cem Concr Compos 2004;26:521–30.
[9] Jayant DM. Health monitoring of civil engineering materials. PhD thesis. Indiana, USA: University of Purdue; 2008. 183p.
[10] Khokhar MIA, Rozière E, Tucry P, Grondin F, Loukili A. Optimisation of mix design of concrete with high content of mineral additions. Cem Concr Compos 2010;32:377–85.
[11] Neville AM. Properties of concrete. New York, USA: John Wiley & Sons; 1995. 844p.
[12] Pal SC, Mukherjec A, Pathak SR. Investigation of hydraulic activity of ground granulated blast furnace slag in concrete. Cem Concr Res 2003;33:1481–6.
[13] Radocea A. Autogenous volume change of concrete at very early age. Mag Concr Res 1998;50:107–13.
[14] Reinhardt H-W, Grosse CU. Continuous monitoring of setting and hardening of mortar and concrete. Construct Build Mater 2004;18:145–54.
[15] Robeyst N, Gruyaert E, Grosse CU, De Belie N. Monitoring the setting of concrete containing blast-furnace slag by measuring the ultrasonic *p*-wave velocity. Cem Concr Res 2008;38:1169–76.
[16] Robeyst N. Monitoring setting and microstructure development in fresh concrete with the ultrasonic through-transmission method. PhD Thesis. Belgium: University of Gent; 2009. 261p.
[17] Rozière E, Granger S, Turcry Ph, Loukili A. Influence of paste volume on shrinkage cracking and fracture properties of self-compacting concrete. Cem Concr Compos 2007;29:626–36.
[18] Rozière E, Loukili A, Cussigh F. A performance based approach for durability of concrete exposed to carbonation. Construct Build Mater 2009;23:190–9.
[19] Slowik V, Schmidt M, Fritzsch R. Capillary pressure in fresh cement-based materials and identification of the air entry value. Cem Concr Compos 2008;30:557–65.
[20] Turcry P, Loukili A. Evolution of plastic shrinkage cracking of self-consolidating concrete. ACI Mater J 2006;4:272–9.
[21] Voigt T, Grosse C, Sun Z, Shah SP, Reinhardt HW. Comparison of ultrasonicwave transmission and reflection measurements with *p*- and *s*-waves on early age mortar and concrete. Mater Struct 2005;38:729–38.